IEEE Access
Multidisciplinary ⋮ Rapid Review ⋮ Open Access Journal

Received 22 May 2023, accepted 5 June 2023, date of publication 9 June 2023,
date of current version 28 December 2023.

Digital Object Identifier 10.1109/ACCESS.2023.3284855

RESEARCH ARTICLE

Ka-Band Tray-Type Spatial Power Combiner Using *H*-Plane Expanded Waveguide With Side-Ridges

SUNGJUN PARK AND JINHO JEONG, (Member, IEEE)
Department of Electronic Engineering, Sogang University, Seoul 04107, South Korea

Corresponding author: Jinho Jeong (jjeong@sogang.ac.kr)

This work was supported by the Samsung Research Funding and Incubation Center of Samsung Electronics under Project SRFC-IT2002-08.

ABSTRACT A tray-type spatial power combiner is proposed at *Ka*-band using an *H*-plane expanded waveguide with side-ridges and a dipole transition array. In order to overcome the small size of the *Ka*-band standard waveguide and accommodate as many as trays (six trays in this work), the *H*-plane of the waveguide is expanded by three times using two-stepped waveguide transition. A circular post is employed to effectively suppress higher-order modes in the expanded waveguide. In addition, a side-ridged waveguide is proposed to reduce non-uniformity in the field and power distribution along the expanded *H*-plane which seriously degrades power combining efficiency. It boosts the electric field close to the waveguide sidewalls by adding the metallic ridges which reduces the waveguide height at the sides. It is shown from the simulation that the proposed side-ridged waveguide can evenly distribute the electromagnetic power and reduce the magnitude imbalances between the trays. In addition, a capacitive iris is introduced in the ridges to improve the phase balance as well. The *H*-plane expanded waveguide with side-ridges was fabricated and the measurement showed an insertion loss as low as 0.2 dB at *Ka*-band. Then, six trays consisting of dipole transition and microstrip line on the dielectric substrate was accommodated between the *H*-plane expanded waveguides with side-ridges. The overall power combining system exhibited the measured insertion loss of 1.2 dB (back-to-back loss) at *Ka*-band. This result belongs to the excellent performance in terms of insertion loss and the number of the trays among the tray-type spatial power combiners reported at *Ka*-band.

INDEX TERMS Expanded waveguide, millimeter-wave, spatial power combiner, waveguide transitions.

I. INTRODUCTION

High output power is a strong requirement for microwave and millimeter-wave communications and radars in both military and commercial applications [1]. Traveling-wave tube amplifiers (TWTAs) have been a good choice for high-power and high-efficiency power sources. In recent years, there has been extensive research replacing TWTAs with solid-state power amplifiers (SSPAs) thanks to the advancement of high-power transistor technologies such as gallium nitride (GaN) high electron mobility transistors (HEMTs). Compared to TWTAs, the SSPAs can allow advantages in terms of reliability, size, weight, and cost [2], [3]. However, output power available from a single SSPA is still very limited, especially at millimeter-wave frequencies, and thus power combining is essential for high-power power generation using a number of SSPAs.

Generally, there exist two power-combining techniques, planar and spatial. A representative planar technique is a corporate power-combiner connecting many two-way couplers like Wilkinson or Lange couplers in a binary tree. Although it is simple and easy to design, its circuit size and loss increase with the number of devices combined, so that it is unsuitable for massive power combination [4], [5]. On the contrary, spatial power combiners maintain high combining-efficiency nearly independent of the number of the devices combined.

The associate editor coordinating the review of this manuscript and approving it for publication was Yiming Huo.

Therefore, they have been widely used for millimeter-wave massive power generations [6].

Millimeter-wave spatial power combiners are commonly designed on the rectangular waveguides which are well-suited for power combining in terms of loss and heat-sinking property. For example, waveguide-based spatial power combiners were proposed at *W*-band using cavity resonances which helped to reduce the combiner size but leaded to a narrow-band operation [7], [8]. Tray-type power combiners, where many trays with power devices are vertically stacked inside the rectangular waveguide, have been widely adopted for high-power generation in several frequency bands. In [9] and [10], several PA trays were spatially combined within *X*-band standard waveguide using a tapered slot antenna array. In both papers, bond-wires were used to convert the TE_{10} mode of the waveguide into the quasi-TEM mode of the microstrip. In [11], a double antipodal finline-to-microstrip transition was proposed to combine two PA trays in the *Ka*-band standard waveguide, exhibiting an excellent combining efficiency. However, the number of the trays was limited to only two because of very small size of *Ka*-band standard waveguide.

To alleviate this problem and accommodate many trays, there have been several approaches to enlarge the size of the waveguide using the tapered and stepped transitions, while maintaining TE_{10} mode without generating higher-order modes [12], [13]. Tapered transition takes use of gradual impedance transformation to achieve broadband return loss. However, it requires a long taper to sufficiently suppress higher-order modes which can lead to the increase in size and insertion loss. In [14], *K*-band waveguide is oversized by ∼3 times using the tapered transition, and TE_{20} mode was effectively suppressed by using a symmetric loading structure. On the other hand, a multi-stepped waveguide transition can be designed in a short length, allowing relatively good return loss and higher-order mode suppression [15]. Stepped waveguide transitions have been widely adopted for the broadband transition between coaxial cables, rectangular waveguides, and microstrip lines [16], [17], [18]. The power combiner using two-stepped waveguide was introduced in [19], where *Ka*-band waveguide was enlarged by ∼1.7 times in both *E*- and *H*-plane to accommodate two dipole-transition trays.

To achieve a high combining efficiency from the tray-type power combiner, it is critical to maintain a good balance in the magnitude and phase of transmission coefficient from input to each tray. However, the electric field (*E*-field) of TE_{10} mode is maximum at the center of *H*-plane and zero at both sidewalls of the waveguide. Then, the trays located close to sidewalls will capture less power than those around center. There can also exist phase imbalances between the trays depending on their location. These imbalances cause the serious degradation in the combining efficiency. In [20] and [21], the dielectric slab was loaded along the sidewall to obtain a uniform field illumination. However, it can cause the increase in insertion loss and complexity in fabrication.

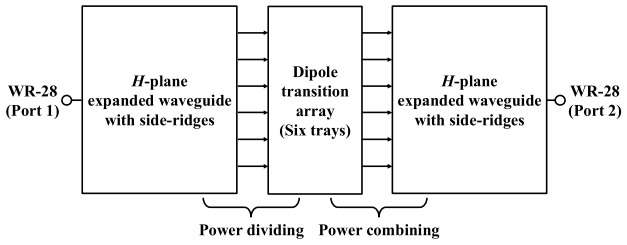

FIGURE 1. Block diagram of tray-type spatial power combiner using the proposed *H*-plane expanded waveguide with side-ridges and dipole transition array (six-trays).

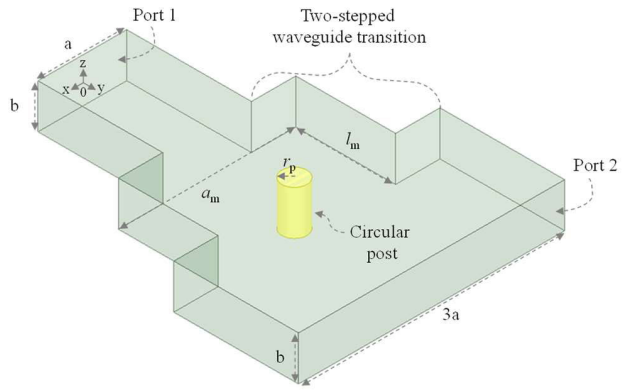

FIGURE 2. *H*-plane expanded waveguide using two-stepped waveguide transition.

In this work, *Ka*-band tray-type spatial power combiner is proposed using an *H*-plane expanded waveguide with side-ridges and a dipole transition array. It can accommodate as many as six trays by expanding the *H*-plane size of *Ka*-band standard waveguide using a two-stepped waveguide transition. A circular post is employed to reduce the generation of higher-order modes. In addition, a side-ridged waveguide with a capacitive iris is proposed to obtain equal power and phase distributions between the six trays which contain waveguide-to-microstrip transition using dipole antenna. The detailed design of the proposed *H*-plane expanded waveguide and dipole transition array is discussed in section II with the electromagnetic (EM) simulations. Fabrication and measurement are described in section III with the performance comparison with previous publications.

II. DESIGN OF TRAY-TYPE SPATIAL POWER COMBINER USING *H*-PLANE EXPANDED WAVEGUIDE

Fig. 1 shows a back-to-back connected power combining system using the proposed *H*-plane expanded waveguides with side-ridges Input (port 1) and output (port 2) are configured in a standard *Ka*-band rectangular waveguide (WR-28) ($a = 7.112$ mm, $b = 3.556$ mm) operating in a dominant mode, TE_{10}.

A. H-PLANE EXPANDED WAVEGUIDE

Fig. 2 shows the designed *H*-plane expanded waveguide which is mirror-symmetrical about the central *E*-plane ($x = 0$). The *H*-plane of the standard waveguide is expanded by three times from a to $3a$ in a two-step. Multi-step higher

than two can also be designed at the expense of the increase in the size and loss. In a two-step expansion, the width (a_m) and length (l_m) of the intermediate waveguide should be determined appropriately, taking into account impedance matching and insertion loss. The waveguide impedance is associated with a_m, which can be determined to achieve broadband impedance matching between the standard and the triple expanded waveguides Initial EM simulations indicate that broadband impedance matching can be achieved for a_m values ranging from $1.5a$ to $2.5a$.

Discontinuities in the H-plane step which can be represented by inductive impedance, may excite higher-order modes that propagate along the expanded waveguide [22]. This is because the cut-off frequency (f_{cmn}) of higher-order modes decreases with increase in width a, as given in (1), and falls into the operating frequency of interest. These higher order modes seriously degrade the transmission performance of the dominant TE_{10} mode [23]

$$f_{cmn} = \frac{1}{2\pi\sqrt{\mu\varepsilon}}\sqrt{\left(\frac{m\pi}{a}\right)^2 + \left(\frac{n\pi}{b}\right)^2} \tag{1}$$

where m and n are integers, representing mode order, μ and ε are the permittivity and permeability of the filling material of the waveguide, respectively. Based on the simulation results of the TE_{30} mode propagation, the width (a_m) of the intermediate waveguide was determined to be $2a$.

There are two discontinuities in the waveguide width which are separated by a distance of l_m, as shown in Fig. 2. If these discontinuities are too close to each other, the higher modes excited at each discontinuity can couple and interact [22]. In this study, l_m was determined to be 8.0 mm (about 0.8 × wavelength at 34 GHz), which was found to be sufficiently distant to induce high attenuation of the TE_{30} mode above 34 GHz, according to the EM simulation. However, it is still necessary to achieve the wider band suppression of higher-order modes There have been research suppressing higher order modes using waveguide filters and absorbers [24], [25] which entail additional machining, bulky size, and extra losses. In this work, a circular post is introduced in the stepped waveguide to effectively suppress the higher-order modes as illustrated in Fig 2.

Fig. 3 demonstrates the simulation results of the H-plane expanded waveguide, depending on the expansion steps and the presence of a post. When a single-step triple expansion (from a to $3a$) is employed in the H-plane, it leads to significant generation and transmission of the TE_{30} mode, as shown by the slotted line in Fig. 3(a), resulting in degradation of the transmission performance of the dominant TE_{10} mode, as depicted in Fig. 3(b). In contrast, a two-step expansion mitigates the generation of the TE_{30} mode, especially at higher frequencies in the *Ka*-band. Furthermore incorporating a circular post in a two-step expanded waveguide effectively reduces the generation of the TE_{30} mode uniformly across the entire *Ka*-band as indicated by the solid line in Fig. 3(a). This enables wideband low-loss transmission of the TE_{10} mode, with a loss of less than 1.0 dB from 29.0 to 38.9 GHz, as illustrated in Fig. 3(b). This improvement comes at the expense of a degradation in the impedance matching bandwidth due to the circular post as demonstrated in Fig. 3(c), where S_{11} remains below −10 dB from 30.1 to 38.1 GHz.

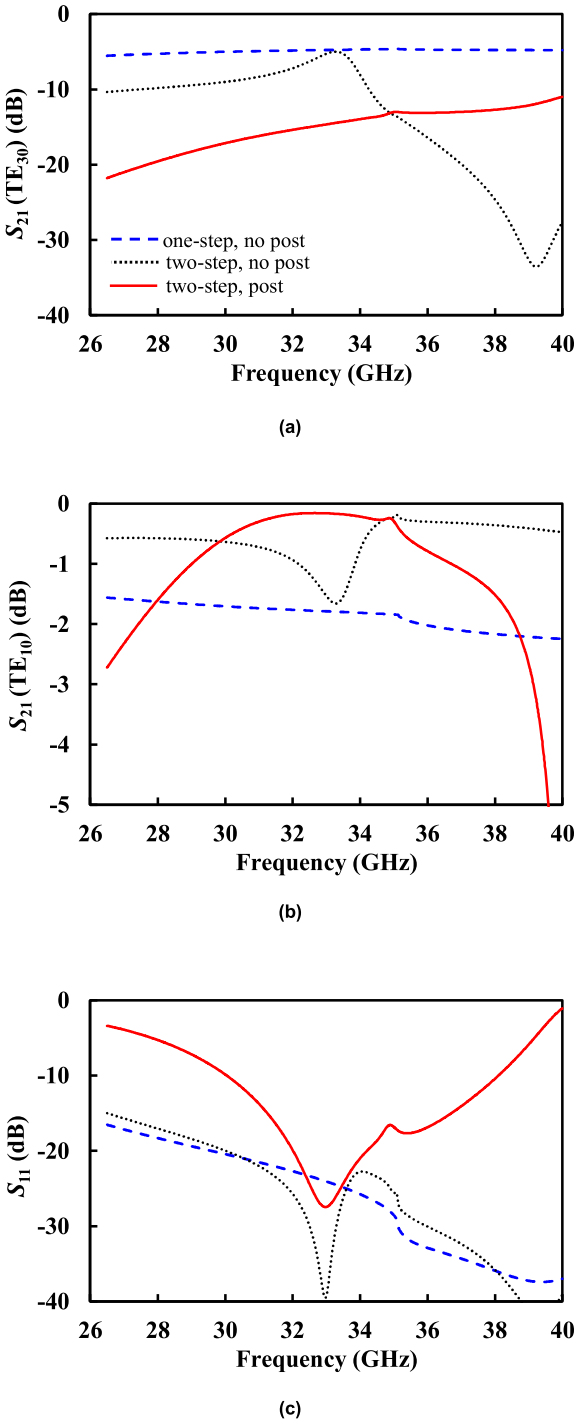

FIGURE 3. Simulated performance of proposed *H*-plane expanded waveguide depending on expansion steps and presence of post. (a) Transmission coefficient of TE_{30} mode. (b) Transmission coefficient of TE_{10} mode. (c) Reflection coefficient.

The circular post serves as a shorting pin and is represented by a small shunt inductance in the model. This configuration

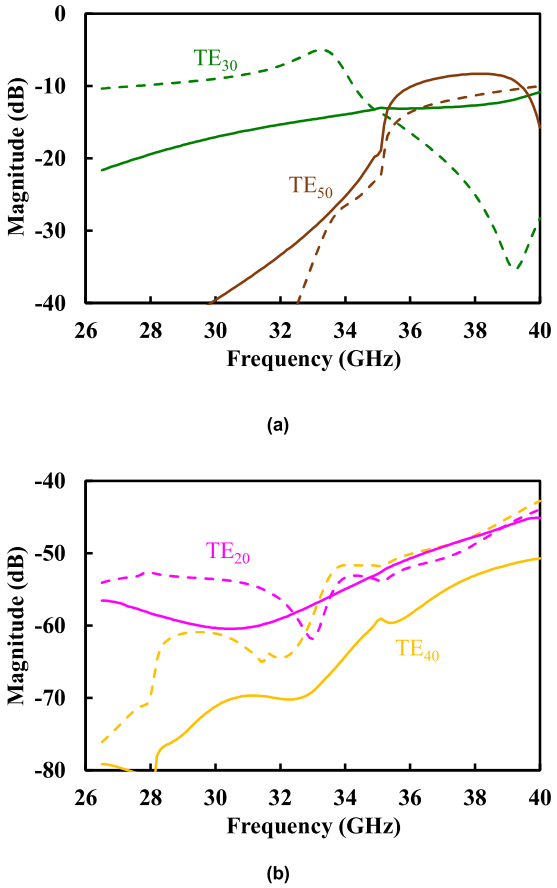

FIGURE 4. Higher-order mode generations in the *H*-plane expanded waveguide depending on the circular post. (a) Odd higher-order modes. (b) Even higher-order modes. Solid: with circular post, dashed: without circular post.

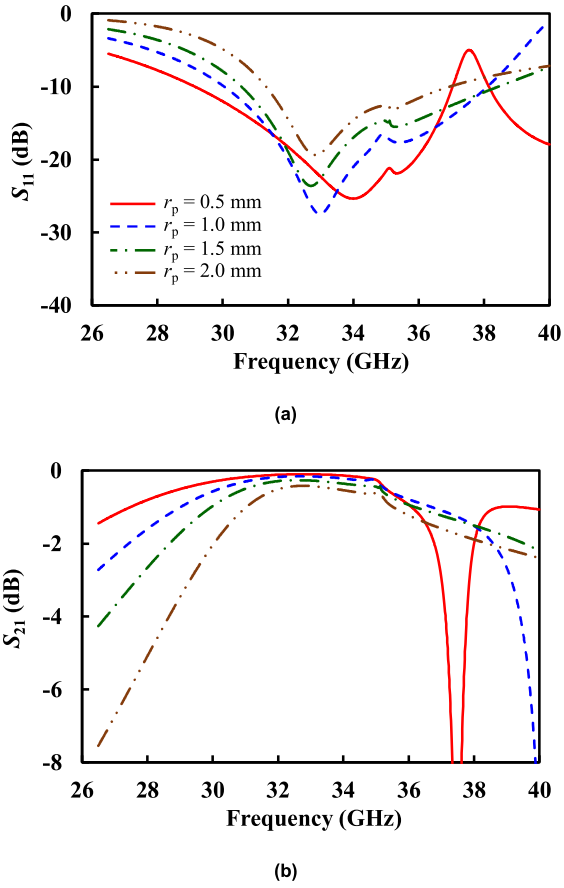

FIGURE 5. Simulated performance of the *H*-plane expanded waveguide as a function of the radius of circular post (a) Reflection coefficient. (b) Transmission coefficient.

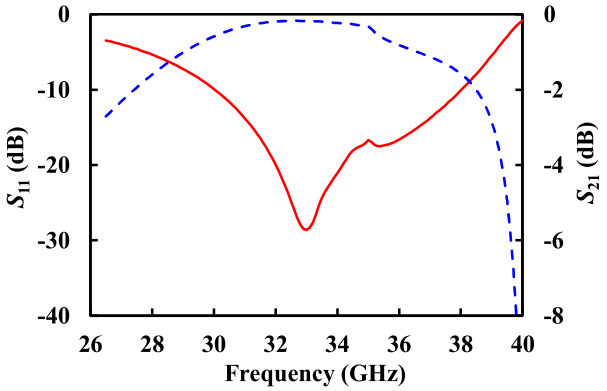

FIGURE 6. Simulated S-parameters of *H*-plane expanded waveguide using two-stepped transition with circular post.

minimizes the electric field at the center of the *H*-plane. This particular characteristic plays a crucial role in preventing the generation and propagation of the TE_{m0} mode with odd m, which typically exhibits a maximum electric field at the center of the *H*-plane. Fig. 4 shows the effect of the circular post on the generation of higher-order modes in the two-stepped waveguide. The radius of the circular post (r_p) is 1.0 mm As compared in Fig. 4(a), the circular post can effectively suppress the TE_{30} mode by more than 168 dB on average from 26.5 to 349 GHz which belongs to the frequency band of interest in this work. The TE_{50} mode exhibits a cut-off frequency f_{c50} of 35.5 GHz according to (1), and its generation is very small at frequencies lower than f_{c50}. Even higher-order modes such as TE_{20} and TE_{40}, are suppressed by more than 40 dB, even in the absence of the circular post. This is because the expanded waveguide is symmetrical about $x = 0$, making it difficult for the incident TE_{10} mode with even symmetry in electric field intensity to generate even-order modes with odd symmetry in electric field intensity.

The radius (r_p) of the circular post has an impact on the bandwidth of both impedance matching and insertion loss, as demonstrated in Fig. 5. As r_p decreases, the bandwidth expands, and when r_p reaches 1.0 mm, a resonance occurs at the band edge (around 40 GHz). Further decreasing the radius results in a shift of the resonant frequency down to 37.5 GHz and a significant degradation of the bandwidth. Taking these observations into account, the value of r_p was chosen to be 1.0 mm.

Fig. 6 shows the simulated *S*-parameters of the designed expanded waveguide using the two-stepped waveguide

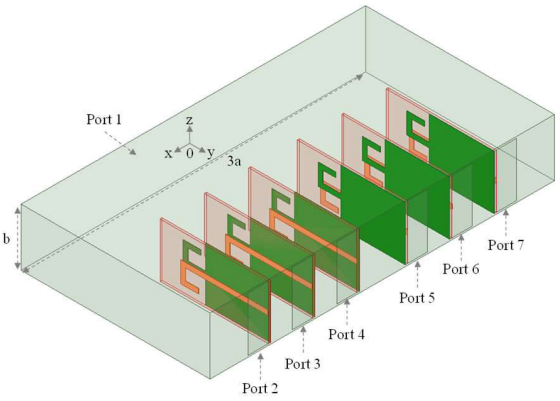

(a)

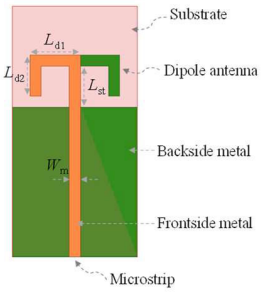

(b)

FIGURE 7. Dipole transition array (six trays) inside the *H*-plane expanded waveguide. (a) Overall view. (b) Layout of the dipole transition.

TABLE 1. Dimensions of the dipole transition (units: mm).

L_{d1}	L_{d2}	L_{st}	W_m
1.3	1.1	1.1	0.3

transition with the circular post. The input return loss remains better than 10 dB from 30. to 38.0 GHz, with an insertion loss below 1.6 dB. The observed increase in insertion loss for frequencies above 35.5 GHz is attributed to the generation of the TE_{50} mode. The simulation results indicate that the conductor loss of the waveguide is negligible, suggesting that the insertion loss of the expanded waveguide is primarily influenced by impedance mismatch and the generation of higher order modes.

In the rectangular waveguide the E-field distribution in TE_{10} mode follows a cosine function of x, that is, it is peak at $x = 0$ (at center) and zero at $x = \pm 1.5a$ (on waveguide sidewall). It implicates that the EM power is non-uniformly distributed between the power combining trays which are located along x-axis (or H-plane).

Fig. 7(a) shows the six trays placed inside the expanded waveguide with an H-plane size of $3a$. Note that the faces of the trays are arranged such that the overall structure maintains symmetry about $x = 0$ (or yz-plane). Each tray consists of a dipole transition and microstrip line on a 127 μm-thick

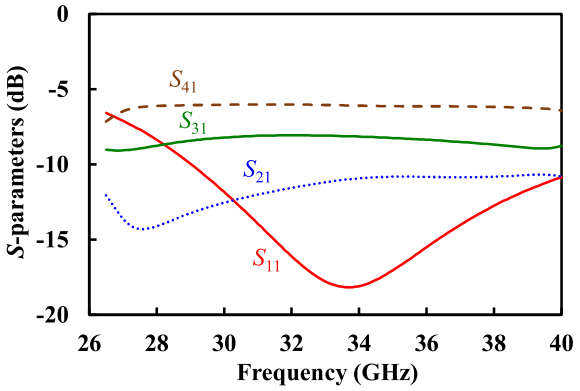

FIGURE 8. Simulated S-parameters of the dipole transition array in the *H*-plane expanded waveguide of Fig. 5(a).

RT Duroid 5880 substrate with dielectric constant of 2.2, as shown in Fig. 7(b). The dipole antenna is approximately half-wave long at the center frequency. The dimensions of the dipole antenna and microstrip line are determined using EM simulations and provided in Table 1. They allow a good transition performance between the standard waveguide and the microstrip line such as insertion loss less than 0.6 dB and return loss better than 10 dB from 28.2 to 40.0 GHz [26]. Based on the simulation results, one of the main factors contributing to the insertion loss of the dipole transition is the conductor loss of the 18-μm-thick copper layer. This conductor loss accounts for approximately 0.3 dB in the frequency range of 32 to 36 GHz. In contrast, the dielectric loss of the substrate can be considered relatively negligible, as it remains below 0.1 dB.

Fig. 8 shows the simulated S-parameters of the dipole antenna array of Fig. 7(a) under the TE_{10} mode excitation at port 1. Input return loss is better than 10 dB from 29.0 to 40.0 GHz. However, it shows a serious magnitude imbalance depending on the location of the tray. As expected, the tray around the center ($x = 0$) captures the highest power (or $|S_{41}|$). On the contrary, the power delivered to the tray close to the waveguide sidewall (or $|S_{21}|$) is much lower. The magnitude imbalance between $|S_{41}|$ and $|S_{21}|$ is as large as 4.8 dB at 34.0 GHz. This magnitude imbalance should be minimized for the power combining applications.

B. SIDE-RIDGED WAVEGUIDE

We proposed a side-ridged waveguide to obtain uniform E-field along H-plane and minimize the magnitude imbalance depending on the tray location. In the side-ridged waveguide, as illustrated in Fig. 9, the waveguide height is reduced by T_s around the waveguide sidewall (W_s) so that the E-field can be boosted. Fig. 10 shows the normalized E-field distribution inside the expanded waveguide as a function of a normalized x-axis, or x/a. It demonstrates that the proposed side-ridged waveguide can provide more uniform E-field distribution along H-plane.

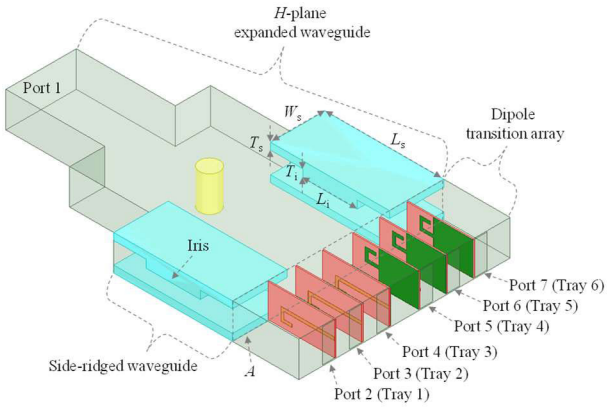

FIGURE 9. Tray-type spatial power combiner using the proposed *H*-plane expanded waveguide with side-ridges and the dipole transition array.

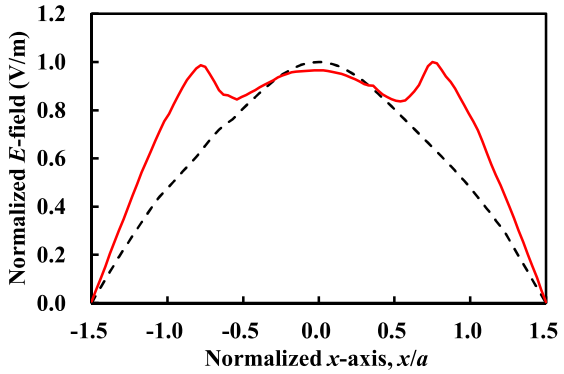

FIGURE 10. Normalized *E*-field distribution inside the expanded waveguide along *H*-plane. Solid: the side-ridged waveguide, dashed: the waveguide without side-ridges.

In addition to the magnitude, the phase balance between the trays is also critical for high-efficiency power combining. In the stepped H plane expanded waveguide, the EM wave exhibits the higher phase velocity around the waveguide sidewall. This leads to the phase difference depending on the x-axis. To reduce the phase imbalance, a capacitive iris is employed in the side-ridged waveguide as shown in Fig. 9. It increases the capacitance of the waveguide around the sidewall, leading to lower cut-off frequency and higher phase constant (β) based on (2) [27]. As a result, the phase velocity in the side-ridged region will become slower, which leads to the reduction in the phase imbalance between the trays.

Fig. 11 demonstrates that the capacitive iris can greatly reduce the phase imbalance between tray 2 and 4 to ±5.3° at 31.0–35.8 GHz.

$$\beta = 2\pi f\sqrt{\mu\varepsilon}\sqrt{1-\left(\frac{f_c}{f}\right)^2} \tag{2}$$

Table 2 shows the optimized dimensions of the H-plane expanded waveguide with side-ridges. Fig. 12 shows the simulated S-parameters of the H-plane expanded waveguide with side-ridges connected to a dipole transition array (the structure in Fig. 9). Input return loss is better than 15 dB

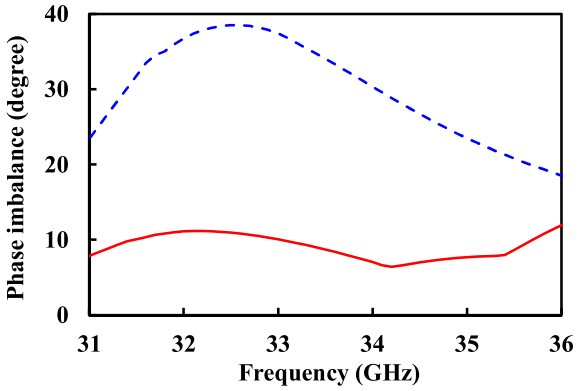

FIGURE 11. Effect of the capacitive iris on the phase imbalance. Solid: with capacitive iris, dashed: without capacitive iris.

TABLE 2. Optimized dimensions of the designed *H*-plane expanded waveguide with side-ridges (units: mm).

a_m	l_m	W_s	T_s	L_s	T_i	L_i
14.224	8.0	5.5	0.7	12.0	0.7	5.5

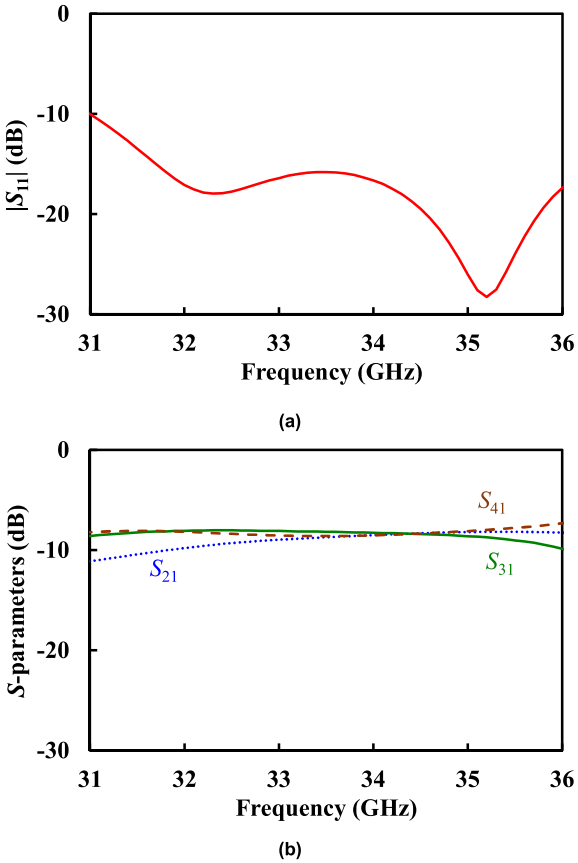

FIGURE 12. Simulated S-parameters of the *H*-plane expanded waveguide with the dipole transition array. (a) Input return loss (S_{11}). (b) Insertion loss.

from 31.7 to 35.8 GHz. Magnitude imbalance is as low as ±1.0 dB in this frequency range. This improvement can be demonstrated by plotting the power distribution on the plane

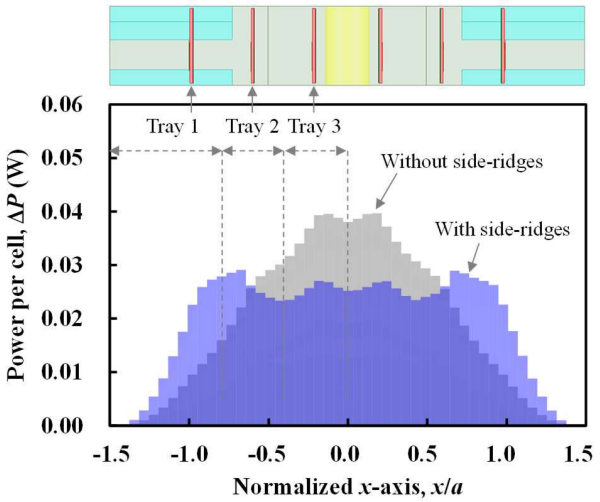

FIGURE 13. Simulated power per cell, ΔP, on the plane A of the H-plane expanded waveguide as a function of the normalized x-axis by a (x/a).

TABLE 3. Power assigned to each tray (P_k) for an input power of 1 W.

Power to each tray	Tray 1	Tray 2	Tray 3
Expanded waveguide without side-ridges	0.06 W	0.15 W	0.28 W
Expanded waveguide with side-ridges	0.16 W	0.16 W	0.17 W

of the side-ridged waveguide output, or the plane A in Fig. 9. It is assumed that 1-W power is applied to port 1. The plane A is equally divided along x-axis into 48 rectangular cells. The EM power on i^{th} cell, ΔP_i, is calculated by the surface integral,

$$\Delta P_i = \int_{A_i} \text{Real}\left\{\vec{S}\right\} \cdot d\vec{A}, \tag{3}$$

where $\vec{S}$ is a Poynting vector (W/m^2) and A_i is the area of the i^{th} cell (m^2). Note that z-dimension or the height of the rectangular cell varies with x. Then, the power incident on k^{th} tray, P_k, is calculated by summing the power on the cells that belong to k^{th} tray.

For example, the tray 1 is placed at $x/a = -1.0$ and captures the powers on the cells from $x/a = -1.5$ to $x/a = -0.8$, as illustrated in Fig. 13. This figure demonstrates that the power in the side-ridged waveguide is more uniformly distributed between the six trays than the expanded waveguide without side-ridges. Table 3 shows the power assigned to each tray (P_k) and demonstrates that the side-ridged waveguide can deliver almost constant power to trays independent of the location.

Fig. 14 shows the simulated S-parameters for the back-to-back connected power combiners with the six trays, or the overall structure of Fig. 1. Input return loss is better than 10 dB from 31.8 to 36.0 GHz where insertion loss is lower

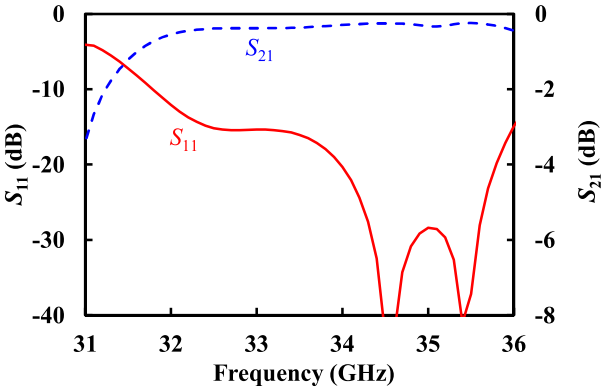

FIGURE 14. Simulated S-parameters of the back-to-back connected power combiner including the dipole transition array.

than 0.7 dB which corresponds to high combining efficiency $> 92.3\%$. Design and simulations were carried out by the full-wave EM simulator, high frequency structure simulator (HFSS) by Ansoft Inc.

III. FABRICATION AND MEASUREMENT

Fig. 15(a) shows the photograph of the back-to-back connected power combiner with overall size of 3.0 cm $\times$ 3.0 cm $\times$ 8.3 cm. It was fabricated in aluminum by a computer-numerical-control (CNC) machining and then was plated with gold. The H-plane expanded waveguide was split along central E-plane as shown in Fig.15(b), and the circular post was packed in the hole. Fig. 15(c) shows the six dipole-transition trays on the five carriers. Each carrier contains a single substrate except for the center carrier which contains two substrates on the front- and back-sides. The substrate was mounted on the carrier using a conductive epoxy.

The performance of the fabricated power combiner was measured using a vector network analyzer (VNA) and *Ka*-band waveguide adaptors. The device-under-test (DUT) was positioned between the WR-28 waveguide adaptors. Prior to measuring the DUT, the measurement setup, including the VNA, cables, and adaptors, was calibrated using the through-reflect-line calibration technique at the reference plane of the waveguides.

Following the calibration, two separate measurements were performed to analyze the characteristics of each block within the power combiner. At first, two H-plane expanded waveguides with side-ridges were directly connected back-to-back without the dipole transition array in between. The measurement results, shown in Fig. 16, indicate that the return loss is higher than 10 dB from 31.2 to 35.0 GHz and that the insertion loss is 0.4 dB on average. This suggests that the loss of the single H-plane expanded waveguide with side-ridges itself is as low as 0.2 dB on average The simulation and measurement results show good agreement, as depicted in the figures.

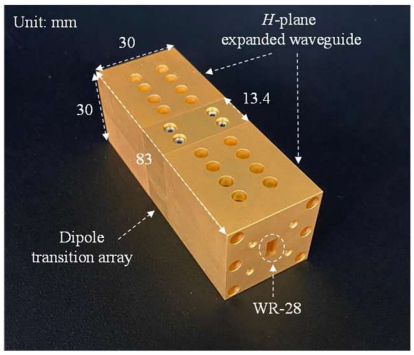

(a)

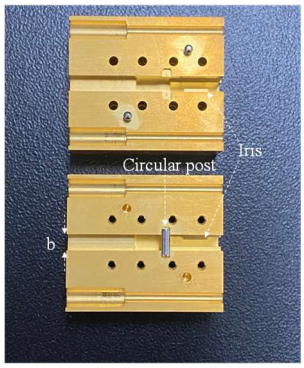

(b)

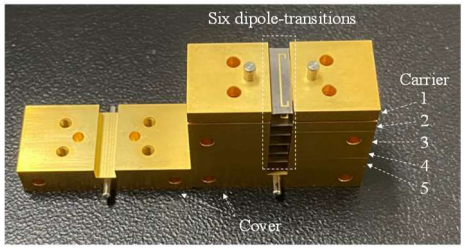

(c)

FIGURE 15. Photograph of the fabricated tray-type spatial power combiner. (a) Overall structure. (b) Internal view of the *H*-plane expanded waveguide. (c) Six dipole-transition trays on the five carriers.

Next, we conducted measurements on the complete power combiner, which includes the dipole transition array consisting of six trays. The measurement results are presented in Fig. 17. The average measured insertion loss within the frequency range of 32.0 to 36.0 GHz is 1.2 dB, while satisfying a return loss of $>$ 10 dB. Compared to the simulation results, the measured loss is approximately 0.8 dB higher. This increased loss in the measurement appears to be attributed to fabrication errors in the dipole transition array. According to the simulation, a misalignment of the dielectric substrates by 100 μm along the y-axis in Fig. 7(a) can result in an additional 0.3 dB loss. Additionally, poor physical contact between the seven-split dipole transition trays may introduce extra loss.

Machining tolerances and surface roughness of the waveguide could also contribute to increased insertion loss.

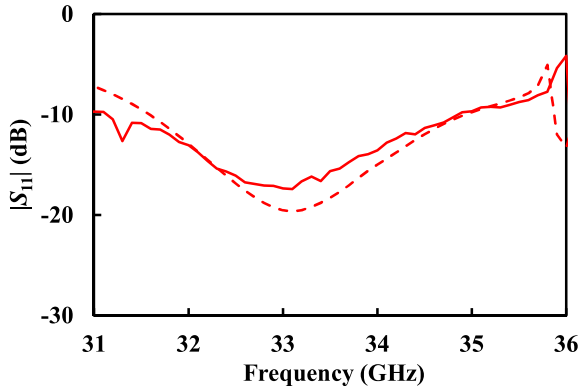

(a)

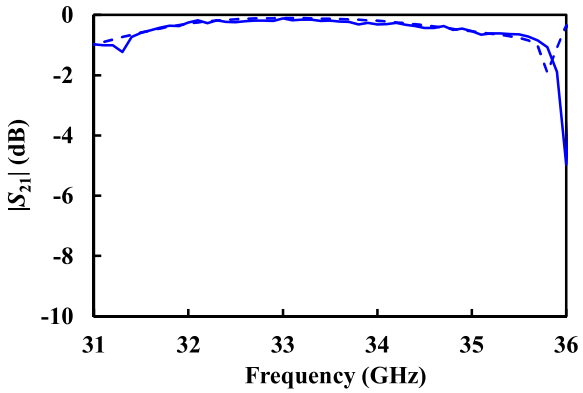

(b)

FIGURE 16. Measured *S*-parameters of the back-to-back connected *H*-plane expanded waveguide without the dipole transition array. (a) Input return loss (S_{11}). (b) Insertion loss (S_{21}). Slotted: simulation, solid: measurement.

Table 4 shows the performance comparison of this work with the previous tray-type spatial power combiners operating from *X*- to *Ka*-band. The power combiners in [9] and, [10] stacks several trays (from two to six) using slotline-to-microstrip transition inside *X*-band standard waveguide without size expansion. In [14] and [19], the *K*- and *Ka*-band waveguides were expanded using stepped and tapered waveguides, so that they could contain six and two trays, respectively. In previous studies [11] and [19], two-tray power combiners were proposed for the *Ka*-band. However, due to the limited size of the *Ka*-band waveguide, it was difficult to accommodate more than two trays. In our study, we addressed this limitation by expanding the standard *Ka*-band waveguide in the *H*-plane. This allowed us to accommodate up to six trays while maintaining low insertion loss or high combining efficiency. To the best of our knowledge, this represents the tray-type power combiner with the largest number of trays stacked in the *H*-plane of the waveguide at the *Ka*-band.

IV. CONLUSION

In this paper, a low-loss tray-type spatial power combiner was proposed at *Ka*-band. The *H*-plane of the standard waveguide

TABLE 4. Performance comparison of the reported tray-type spatial power combiners from *X*- to *Ka*-band.

Reference	Frequency band	Waveguide expansion	Transition type	Number of trays	Range (GHz)	Return loss (dB)	Insertion loss* (dB)	
							Range	Average
[9]	*X*-band	-	Slotline-to-microstrip	4	8.2–12.4	≥ 15	-	-
[10]	*X*-band	-	Slotline-to-microstrip	2	8.2–12.4	≥ 14	1.1–1.7	-
				6	8.2–12.4	≥ 7.5	1.3–2.4	-
[11]	*Ka*-band	-	Finline-to-microstrip	1	26.5–40.0	≥ 17	≤ 0.6	-
				2	22.0–40.0	≥ 10	2.0	1.8
[14]	*K*-band	Tapered waveguide	Tapered-slot antenna	6	18.0–22.0	≥ 14	-	≤ 2.5
[19]	*Ka*-band	Stepped waveguide	Dipole antenna	2	31.6–35.7	≥ 10	≤ 1.0	-
This work	*Ka*-band	Stepped waveguide	Dipole antenna	6	32.0–36.0	≥ 10	1.1–1.6	1.2

*back-to-back connection

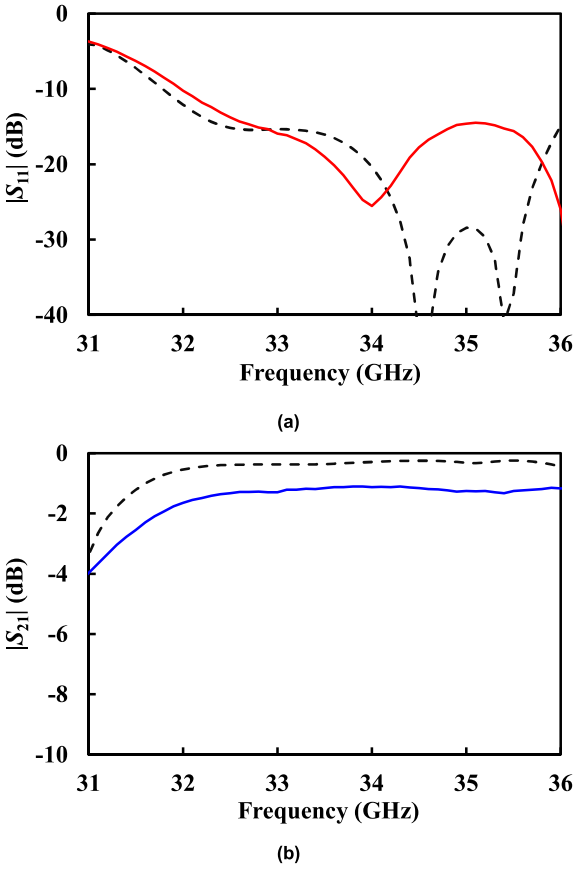

FIGURE 17. Measured *S*-parameters of the back-to-back connected *H*-plane expanded waveguide including the dipole transition array. (a) Input return loss (S_{11}). (b) Insertion loss (S_{21}). Slotted: simulation, solid: measurement.

was expanded by three times using two-step transition to accommodate as many as six dipole-transition trays. The side-ridged waveguide with the capacitive iris was proposed to accomplish uniform power and phase distribution between the six trays to achieve high combining efficiency. In the back-to-back measurement the proposed *H*-plane expanded waveguide with side-ridges exhibited very low loss at *Ka*-band and it could successfully accommodate six dipole-transition trays. Therefore, it can be effectively utilized for *Ka*-band massive power-combining applications. In addition, we expect that the proposed techniques can be applied to further expand the waveguide size to accommodate more active trays while maintaining uniform power distribution.

REFERENCES

[1] K. Song, Y. Fan, and Z. He, "Broadband radial waveguide spatial combiner," *IEEE Microw. Wireless Compon. Lett.*, vol. 18, no. 2, pp. 73–75, Feb. 2008.

[2] W. Q. Lohmeyer, R. J. Aniceto, and K. L. Cahoy, "Communication satellite power amplifiers: Current and future SSPA and TWTA technologies," *Int. J. Satell. Commun. Netw.*, vol. 34, no. 2, pp. 95–113, Mar. 2016.

[3] M. Casto, M. Lampenfeld, P. Jia, P. Courtney, S. Behan, P. Daughenbaugh, and R. Worley, "100 W X-band GaN SSPA for medium power TWTA replacement," in *Proc. WAMICON Conf.*, Clearwater Beach, FL, USA, Apr. 2011, pp. 1–4.

[4] J. Li, L. Li, L. Lu, H. Shi, H. Huo, and A. Zhang, "Four-way waveguide power divider design for W-band applications," *Int. J. RF Microw. Comput.-Aided Eng.*, vol. 28, no. 5, Jun. 2018, Art. no. e21242.

[5] L. W. Epp, D. J. Hoppe, A. R. Khan, and S. L. Stride, "A high-power Ka-band (31–36 GHz) solid-state amplifier based on low-loss corporate waveguide combining," *IEEE Trans. Microw. Theory Techn.*, vol. 56, no. 8, pp. 1899–1908, Aug. 2008.

[6] K. Chang and C. Sun, "Millimeter-wave power-combining techniques," *IEEE Trans. Microw. Theory Techn.*, vol. MTT-31, no. 2, pp. 91–107, Feb. 1983.

[7] L. A. Samoska, M. Taylor, J. Velazco, A. Fung, R. Lin, A. Peralta, and R. Gawande, "A W-band spatial power-combining amplifier using GaN MMICs," in *Proc. 15th Eur. Radar Conf. (EuRAD)*, Sep. 2018, pp. 329–332.

[8] J. Velazco, L. Samoska, M. Taylor, A. Pereira, A. Fung, R. Lin, and A. Peralta, "Spatial power combiner using cavity modes in W-band," in *IEEE MTT-S Int. Microw. Symp. Dig.*, Boston, MA, USA, Jun. 2019, pp. 991–994.

[9] N.-S. Cheng, A. Alexanian, M. G. Case, D. B. Rensch, and R. A. York, "40-W CW broad-band spatial power combiner using dense finline arrays," *IEEE Trans. Microw. Theory Techn.*, vol. 47, no. 7, pp. 1070–1076, Jul. 1999.

[10] N.-S. Cheng, P. Jia, D. B. Rensch, and R. A. York, "A 120-W X-band spatially combined solid-state amplifier," *IEEE Trans. Microw. Theory Techn.*, vol. 47, no. 12, pp. 2557–2561, Dec. 1999.

[11] J. Jeon, Y. Kwon, S. Lee, C. Cheon, and E. A. Sovero, "1.6- and 3.3-W power-amplifier modules at 24 GHz using waveguide-based power-combining structures," *IEEE Trans. Microw. Theory Techn.*, vol. 48, no. 12, pp. 2700–2708, Dec. 2000.
[12] K. Niwa, K. Sakakibara, and N. Kikuma, "Design of spatial power combining circuit using taper waveguide for high-power generation in terahertz band," in *Proc. Int. Symp. Antennas Propag. (ISAP)*, Busan, (South) Korea, Oct. 2018, pp. 1–2.
[13] K. Song, G. Li, Q. Duan, S. Hu, and Y. Fan, "Millimeter-wave waveguide-based out-of-phase power divider/combiner using microstrip antenna," *AEU-Int. J. Electron. Commun.*, vol. 68, no. 12, pp. 1234–1238, Dec. 2014.
[14] L.-Y.-V. Chen and R. A. York, "Development of K-band spatial combiner using active array modules in an oversized rectangular waveguide," in *IEEE MTT-S Int. Microw. Symp. Dig.*, Boston, MA, USA, Jun. 2000, pp. 821–824.
[15] J. Deng and Q. Wang, "A novel compact oversized rectangular waveguide transition based on quadruple-ridged waveguide for millimeter wave applications," *J. Infr., Millim., Terahertz Waves*, vol. 41, no. 7, pp. 776–784, Jun. 2020.
[16] R. V. Gatti, R. Rossi, and M. Dionigi, "In-line stepped ridge coaxial-to-rectangular waveguide transition with capacitive coupling," *Int. J. RF Microw. Comput.-Aided Eng.*, vol. 29, no. 3, 2018, Art. no. e21626.
[17] Y. Wei, C. Arnold, and J. Hong, "A K/Ka-band reconfigurable substrate integrated coaxial line to waveguide transition technology," *IEEE Access*, vol. 10, pp. 65037–65043, 2022.
[18] A. K. Nayak and A. Patnaik, "Design and testing of a broadband microstrip-SIW transition," in *Proc. IEEE Microw. Theory Techn. Wireless Commun. (MTTW)*, vol. 1, Oct. 2020, pp. 91–95.
[19] K. Song, F. Zhang, S. Hu, and Y. Fan, "Millimetre-wave quasi-optical low-loss power combiner based on dipole antenna," *Electron. Lett.*, vol. 49, no. 18, pp. 1160–1162, Aug. 2013.
[20] A. Alexanian and R. A. York, "Broadband spatially combined amplifier array using tapered slot transitions in waveguide," *IEEE Microw. Guided Wave Lett.*, vol. 7, no. 2, pp. 42–44, Feb. 1997.
[21] M. A. Ali, S. C. Ortiz, T. Ivanov, and A. Mortazawi, "Analysis and measurement of hard-horn feeds for the excitation of quasi-optical amplifiers," *IEEE Trans. Microw. Theory Techn.*, vol. 47, no. 4, pp. 479–487, Apr. 1999.
[22] A. Weisshaar, M. Mongiardo, A. Tripathi, and V. K. Tripathi, "CAD-oriented fullwave equivalent circuit models for waveguide components and circuits," *IEEE Trans. Microw. Theory Techn.*, vol. 44, no. 12, pp. 2564–2570, Dec. 1996.
[23] D. M. Pozar, *Microwave Engineering*, 4th ed. New York, NY, USA: Wiley, 2011.
[24] S. Ceccuzzi, C. Ponti, G. L. Ravera, and G. Schettini, "Physical mechanisms and design principles in mode filters for oversized rectangular waveguides," *IEEE Trans. Microw. Theory Techn.*, vol. 65, no. 8, pp. 2726–2733, Aug. 2017.
[25] A. K. Fahad, R. CunJun, T. U. Haq, S. Khan, and M. F. Shahzad, "High power low-loss terahertz filter with higher-order mode suppression," in *Proc. 16th Int. Bhurban Conf. Appl. Sci. Technol. (IBCAST)*, Islamabad, Pakistan, Jan. 2019, pp. 985–988.
[26] S. Park, B. Kang, and J. Jeong, "A broadband radial power combiner using a dipole antenna-based TM mode transducer," *IEEE Access*, vol. 10, pp. 111901–111908, 2022.
[27] M. F. Shah, "Design and analysis of multiple ridge waveguide for wide-band application," in *Proc. IEEE Int. Conf. Adv. Commun., Control Comput. Technol.*, Ramanathapuram, India, May 2014, pp. 886–890.

SUNGJUN PARK received the B.S. degree in electrical engineering from Hoseo University, Asan, South Korea, in 2021. He is currently pursuing the M.S. degree in electronic engineering with Sogang University, Seoul, South Korea. His research interest includes microwave/millimeter-wave power-combining technology.

JINHO JEONG (Member, IEEE) received the B.S., M.S., and Ph.D. degrees in electrical engineering from Seoul National University, Seoul, South Korea, in 1997, 1999, and 2004, respectively. From 2004 to 2007, he was with the University of California at San Diego, La Jolla, CA, USA, as a Postdoctoral Scholar, where he was involved with the design of high efficiency and high-linearity RF power amplifiers. In 2007, he joined the Department of Electronics and Communications Engineering, Kwangwoon University, Seoul, South Korea. Since 2010, he has been with the Department of Electronic Engineering, Sogang University, Seoul. His research interests include monolithic microwave integrated circuits, THz integrated circuits, high-efficiency/high-linearity power amplifiers and oscillators, and wireless power transfers.